Materials Transactions, Vol. 57, No. 4 (2016) pp. 533 to 538

Real Hydrostatic Pressure in High-Pressure Torsion Measured by Bismuth Phase Transformations and FEM Simulations

Kaveh Edalati[1,2,*], Dong Jun Lee[3], Takashi Nagaoka[2], Makoto Arita[2], Hyoung Seop Kim[4], Zenji Horita[1,2] and Reinhard Pippan[5]

[1]*WPI, International Institute for Carbon-Neutral Energy Research (WPI-I2CNER), Kyushu University, Fukuoka 819–0395, Japan*
[2]*Department of Materials Science and Engineering, Faculty of Engineering, Kyushu University, Fukuoka 819–0395, Japan*
[3]*Commercialization Research Division, Korea Institute of Materials Science (KIMS), Changwon 641–831, South Korea*
[4]*Department of Materials Science and Engineering, Pohang University of Science and Technology, Pohang 790–784, South Korea*
[5]*Erich Schmid Institute of Materials Science, Austrian Academy of Sciences, Jahnstrasse 12, 8700 Leoben, Austria*

Hydrostatic pressure is a significant parameter influencing the evolution of microstructure and phase transformations in the high-pressure torsion (HPT) process. Currently, there are significant arguments relating to the magnitude of the real hydrostatic pressure during the process. In this study, phase transformations in bismuth, copper and titanium combined with the finite element method (FEM) were employed to determine the real pressure in processing disc samples by HPT. Any break in the variation of steady-state hardness (monitored experimentally by *in-situ* torque and temperature rise measurements) versus pressure was considered as a phase transition. FEM simulations show that the hydrostatic pressure is reasonably isotropic but decreases with increasing distance from the disc center and remains unchanged across the disc thickness. Both experiments and simulations indicate that the mean hydrostatic pressure during HPT processing closely corresponds to the compressive load over the disc area plus the contact area between the anvils. [doi:10.2320/matertrans.M2015374]

(Received October 2, 2015; Accepted January 18, 2016; Published March 25, 2016)

Keywords: *high-pressure torsion (HPT), severe plastic deformation (SPD), finite element method (FEM), ultrafine-grained (UFG) materials, omega phase*

1. Introduction

The application of high-pressure torsion (HPT) to different kinds of metallic materials[1–4] and ceramics[5,6] is now a well-known procedure for producing significant grain refinement[1–4] and controlling allotropic phase transformations[7–10]. Strain, strain rate, temperature and pressure are four critical parameters that influence the evolution of microstructure and/or phase transformations in HPT processing[4].

Since the earlier works by Bridgman in 1935[11], a general question concerns the real levels of temperature and pressure in processing by HPT. Although recent studies using experimental measurements and the finite element method (FEM) simulations provided reliable results regarding the magnitude of real temperature[12,13], there are significant arguments on the magnitude of real hydrostatic pressure during HPT processing and its significance on microstructures and phase transformations.

Bridgman divided the compressive load by the total area of the sample after deformation and calculated the pressure[11]. Although the capacity of hydraulic press of his HPT facility was 75 tons, he increased the pressure not to more than 5 GPa using the tool steel anvils[11] and not to more than 10 GPa using the tungsten carbide anvils[14]. He suggested that it is possible to attain mean hydrostatic pressures 2–3 times higher than the normal strength of the anvils[15]. Following the Bridgman's works, several groups attempted to increase the pressure up to 50 GPa[16], 25 GPa[17], 20 GPa[18] and 40 GPa[19,20]. However, as discussed in a recent review paper[21], the estimated pressure in these studies may not represent the real pressure, because they calculated the pressure as load over the initial area of the disc. In practice, in order to increase the pressure above 10 GPa in HPT processing, rotational diamond anvil cell or shear diamond anvil cell facilities should be employed[6,22,23].

An inspection of past publications on HPT processing indicates that the estimated pressures are significantly inconsistent. For example, it is well known that pure Ti exhibits a phase transformation from the α phase to the ω phase under 2–3 GPa[24]. The possibility of this phase transformation was first reported by Bridgman in 1948 under pressures higher than 3.5 GPa[25] and later confirmed by Jamieson in 1963[26]. The formation of ω phase after processing by HPT was detected under 2.5–3 GPa by Zilbershtein *et al.*[27], under 4 GPa by Kilmametov *et al.*[28], under 5 GPa by Edalati *et al.*[19] and Todaka *et al.*[29] and under 6 GPa by Shirooyeh *et al.*[30] Sergueeva *et al.*[31] did not detect the ω phase under 5 GPa, Chen *et al.*[32] and Wang *et al.*[33] did not detect the ω phase even under 6 GPa. Although one reason for these inconsistencies can be due to the effect of impurities on the formation of ω phase[34], the current authors found, although unpublished, that the nominal transition pressure can be varied between 4 GPa to 6 GPa depending on the geometry of the anvils even for the same Ti sample.

The present study was thus initiated to determine the real hydrostatic pressure in HPT processing by means of experimental measurements and FEM simulations. Three model metals (Bi, Cu and Ti) were selected and the phase transformations in Bi under pressures of 2.5 GPa (from Bi-I with the rhombohedral crystal structure to Bi-II with the monoclinic crystal structure) and 2.7 GPa (from Bi-II to Bi-III with the tetragonal or orthorhombic crystal structure)[35] were used for calibration of real pressure. Since Bi-II is a hard phase[11], *in-situ* toque and temperature measurements were conducted to detect the formation of Bi-II (both torque and temperature

*Corresponding author, E-mail: kaveh.edalati@zaiko6.zaiko.kyushu-u.ac.jp

rise during HPT processing are proportional to the hardness increase[11,12]).

2. Experimental Materials and Procedures

The HPT facility employed in this study had one upper anvil and one lower anvil made from tool steel (see Fig. 1 for detailed design of the anvils). Flat-bottom holes of 10 mm diameters, 0.25 mm depths and 45° inclination angle at the lateral wall were machined into the center of each anvil. The width of the contact area between the two anvils, where a burr is formed, was 1.5 mm.

The experiments were performed using disc samples of high-purity Bi (99.99%), Cu (99.99%) and Ti (99.9%) with 10 mm diameters and 0.8 mm thicknesses. The discs were annealed for 1 h at 493 K for Bi, 873 K for Cu and 1073 K for Ti. In order to reduce the grain sizes to the steady states and achieve saturation levels of hardness, each disc was compressed between the upper and lower anvils under a load of 150 kN. The lower anvil was then rotated for $N = 5$ turns with respect to the upper anvil at room temperature ($T_o = 301.4$ K) with a rotation speed of $\omega = 1$ rpm. The microstructure of the HPT-processed Bi was examined using optical microscopy and the microstructures of the HPT-processed Cu and Ti were examined using transmission electron microscopy (see Refs. 19,36) for details of TEM sample preparation). Vickers microhardness of the discs at different distances from the center was measured using a load of 50 g for Bi and 200 g for Cu and Ti.

Following the initial processing of samples for $N = 5$ turns under a load of 150 kN, the load was first released to 24.5 kN and subsequently increased to 490 kN with 24.5 kN increments. The samples were processed for $N = 0.5$ turns under each load and their behavior was evaluated by *in-situ* torque measurements using strain gauges placed on the upper anvil and by temperature measurements using a well-calibrated K-type thermocouple located at the rotation axis at 10 mm away from the disc surface. Note that the samples were cooled down to room temperature after termination of rotation under each selected load.

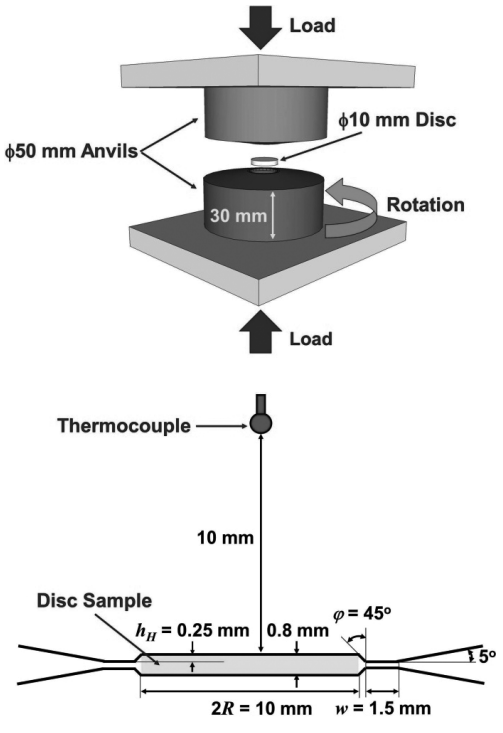

Fig. 1 Schematic illustration of HPT facility.

3. Calculation Methods

The FEM simulations were employed using the rigid-plastic FEM package, DEFORM-3D ver. 6.1 (see Ref. 37) for details). The geometry of the modeled anvils and disc specimens was the same as the experimental geometry used in this study. The model consisted of 150,000 meshes. Plastic deformation was simulated by (i) compression with a speed of 0.1 mm/s under the loads of 50, 150, 245 and 340 kN, and (ii) torsion with a rotation speed of 1 rpm for $N = 1$ turn. It should be noted the effect of strain rate on stress was not simulated in this study. However, since the stress-strain relationship used in the FEM simulations (see Ref. 37)) was achieved using a compression speed of 0.1 mm/s and a rotation speed of 1 rpm, the same processing conditions were simulated in this study.

Since the surface of both sample and anvils were roughened (to ~30 μm roughness) before the HPT process to increase the friction and to avoid the slippage between the sample and the anvils, the slippage between the sample and anvils was ignored in the simulations, i.e. sticking condition was used. The deformation of anvils during the process was not taken into account, i.e. the anvils were considered as rigid.

4. Results and Discussion

Figure 2 shows the variation of (a) torque and (b) temperature for samples processed by HPT under a load of 150 kN for up to $N = 5$ turns. The torque increases with increasing the number of turns and reaches steady states after $N = 2$–5 turns. No torque peak appears in Bi and Cu but a torque peak appears in Ti because of texture development (slip planes becomes parallel to the disc surface in Ti[19]). When the slip planes are oriented in a direction parallel to the disc surface, the shear flow stress will increase in the pressing direction, but the flow stress decreases in the rotation (torque) direction. The temperature also increases with increasing the number of turns, but the rate of temperature rise significantly decreases with increasing the number of turns, in agreement with Ref. 12). Both torque and temperature rise become more significant as the melting temperature increases (melting temperature: 544 K for Bi, 1358 K for Cu and 1941 K for Ti).

It should be noted that the temperatures in this study were measured in the upper HPT anvil at 10 mm away from the sample, as shown in Fig. 1. In an attempt to measure the real temperature of samples, a thermocouple was directly placed between a Cu disc and upper anvil and the temperature was directly measured during the HPT process (this experiment was recommended by Prof. Alexander P. Zhilyaev of Russian Academy of Science). Figure 3 compares the real temperature of the sample and the temperature of anvil at 10 mm away from the disc surface. It is apparent that the temperature rise in the sample after $N = 1/3$ turns is 7 K, while the tem-

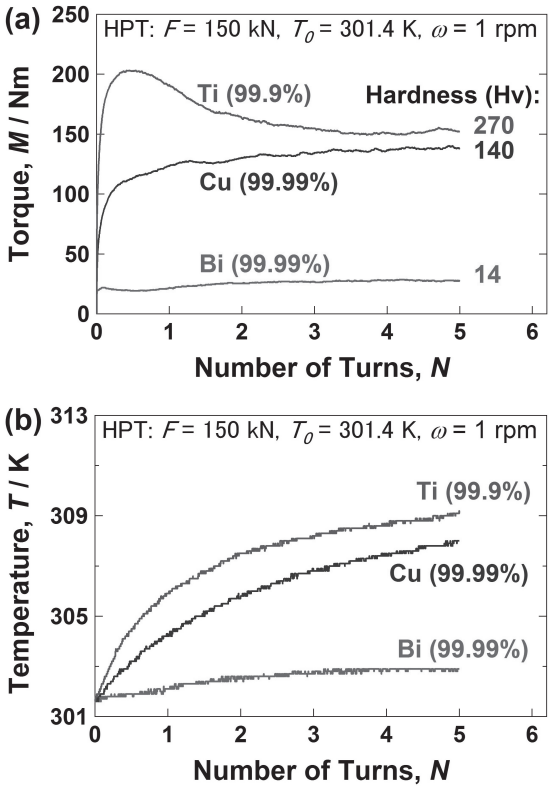

Fig. 2 Variation of (a) torque and (b) temperature against number of turns for Bi, Cu and Ti processed by HPT for $N = 5$ turns under load of 150 kN. Levels for steady-state hardness are given in (a).

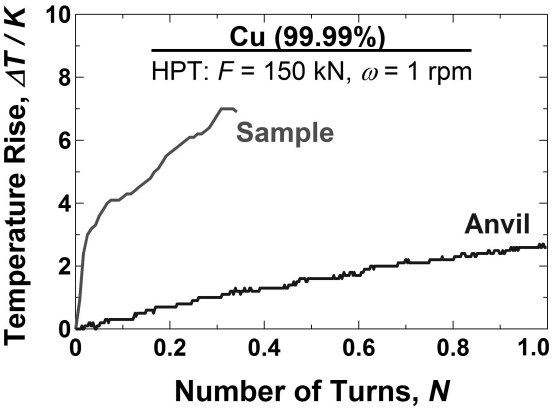

Fig. 3 Variation of temperature rise against number of turns experimentally measured by placing thermocouples on upper surface of disc and in anvil at 10 mm away from disc surface for Cu processed by HPT for $N = 1$ turn under load of 150 kN (thermocouple which was placed on disc surface broke after $N = 1/3$ turns).

perature rise in the anvil is 1.3 K (the thermocouple broke after $N = 1/3$ turns). These results are in good agreement with an earlier publication of the authors[12], which suggested that the temperature rise in Cu processed under a nominal pressure of 2 GPa with a rotation speed of 1 rpm should be 6 K. The small difference between the results presented in Fig. 3 and those reported in Ref. 12) is due to the small difference in the total contact area between the two anvils in these two studies.

Figure 4 shows the variations of torque against the number of turns achieved by experimental measurements and FEM

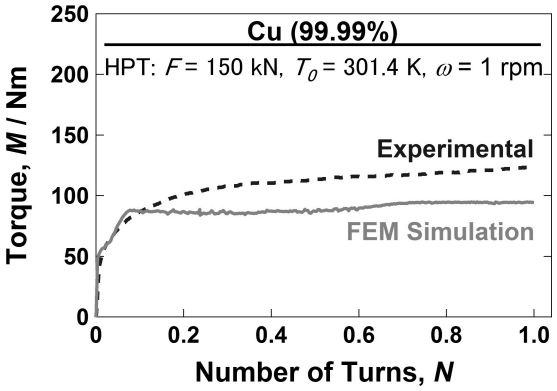

Fig. 4 Variation of torque against number of turns obtained by experiments and FEM simulations for Cu processed by HPT for $N = 1$ turn under load of 150 kN.

Table 1 Vickers microhardness and grain size for Bi, Cu and Ti samples after annealing and after HPT processing up to steady state.

Metals	Microhardness, HV / kg.mm^{-2}		Grain Size, d / μm	
	Anneal	HPT	Anneal	HPT
Bi (99.99%)	10	14	1000	20
Cu (99.99%)	50	140	150	0.3
Ti (99.9%)	140	270	230	0.2

simulations for samples processed by HPT under a load of 150 kN for up to $N = 1$ turn. It is apparent that torque levels achieved by experiments and FEM simulations are reasonably consistent, although the experimental torque value is slightly higher than the calculated one. The uncertainty on what really happen in the contact area between the two anvils (where a burr is formed) should be the main reason for the discrepancies between the simulated and measured torque values.

Table 1 documents the microhardness and grain size for Bi, Cu and Ti after annealing and after processing by HPT to the steady state. The hardness increases and the grain size decreases after processing by HPT for the three metals. The steady-state hardness reaches 14, 140 and 270 Hv and the steady-state grain size reaches 20, 0.3 and 0.2 μm for Bi, Cu and Ti, respectively. Both hardening and grain refinement become more significant as the melting temperature of the metals increases, in accordance with Ref. 38). Detailed information regarding the evolutions of hardness and microstructure are given in the Appendix for Bi, Ref. 36) for Cu and Ref. 19) for Ti.

Figure 5 plots (a) torque rise and (b) temperature rise as a function of applied compressive load. For Cu, which exhibits no phase transformation, both steady-state torque and temperature increase monotonically with increasing the load. For Bi, which exhibits a phase transformation from a soft Bi-I phase to a hard Bi-II phase under a pressure of 2.5 GPa[11,34], both torque and temperature increase significantly under a load of 320 kN. This observation indicates that the mean hydrostatic pressure under a load of 320 kN should be ~2.5 GPa. Both torque and temperature decrease with increasing the load to more than 320 kN because of a transition from the Bi-II phase to a soft Bi-III phase under a pressure of 2.7 GPa[35].

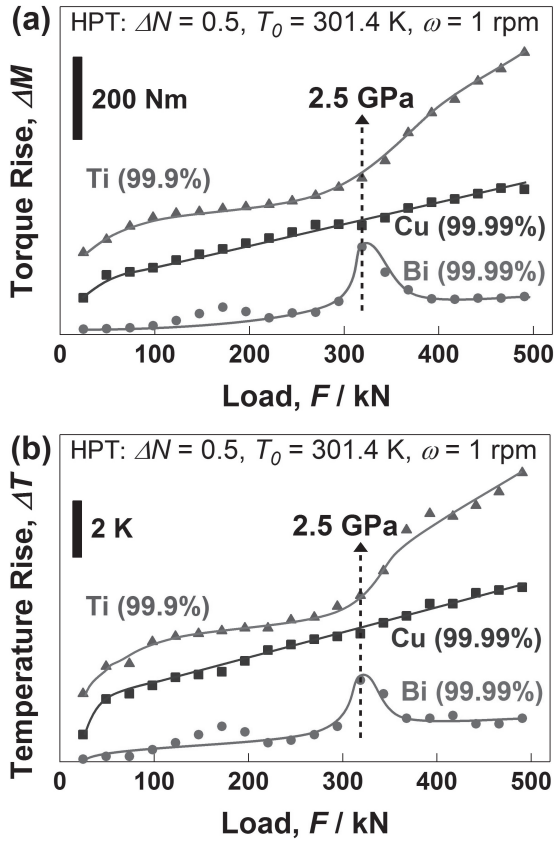

Fig. 5 Variation of (a) torque rise and (b) temperature rise against load for Bi, Cu and Ti processed by HPT. Samples were first processed for $N = 5$ turns under load of 150 kN and subsequently processed for $N = 0.5$ turns under selected loads.

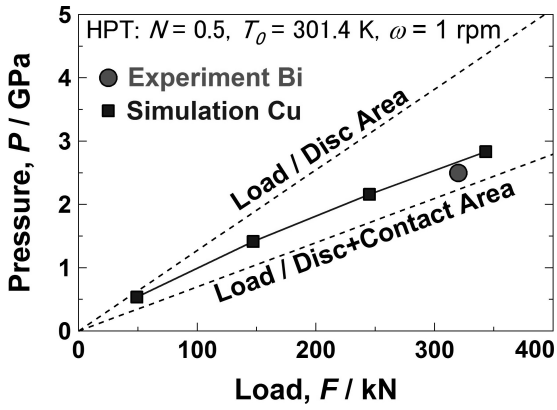

Fig. 6 Plots of hydrostatic pressure against load obtained by experiments using Bi and FEM simulations using Cu. Dotted lines shows levels of pressure calculated as load over area of disc (upper line) and load over area of disc plus contact area between two anvils (lower line).

For Ti, which exhibits an $\alpha \rightarrow \omega$ phase transformation under a pressure of 2–3 GPa[24], a break in the variations of torque and temperature versus load is visible under a load of 320 kN. This indicates that a transition to a hard ω phase should have occurred under a hydrostatic pressure of ~2.5 GPa in Ti.

The current experimental results, as summarized in Fig. 6, indicate that if the pressure is estimated as load over the initial area of disc, the pressure will be significantly overestimated (4.1 GPa for 320 kN). However, if pressure is estimated as load over the total area of disc and contact region, the pressure can be estimated with a reasonable error (2.2 GPa for 320 kN). The results of FEM simulations, as shown in Fig. 6, are reasonably consistent with the experimental results using Bi, suggesting that the pressure should not be estimated as load over the area of flat-bottom hole on the anvils, $F/\pi R^2$, but over the total area including the contact area between the two anvils, $F/\pi(R + h_H \tan\varphi + w)^2$, where a burr is formed (F: Load, R: disc radius, h_H: depth of flat-bottom hole, φ: inclination angle at lateral wall of hole, w: width of burr region). Introducing κ as a factor for the overestimation, the value of κ may be evaluated through the following relation:

$$\kappa = (R + h_H \tan\varphi + w)^2 / R^2. \quad (1)$$

For the present case, $R = 5$ mm, $w = 1.5$ mm, $h_H = 0.25$ mm and $\varphi = 45^\circ$, it follows that $\kappa = 1.8$. It is suggested that the overestimation is reasonably assessed through κ, when considering the past publications where the pressures for the transformation to the ω phase in Ti and Zr are invariably high[19,20].

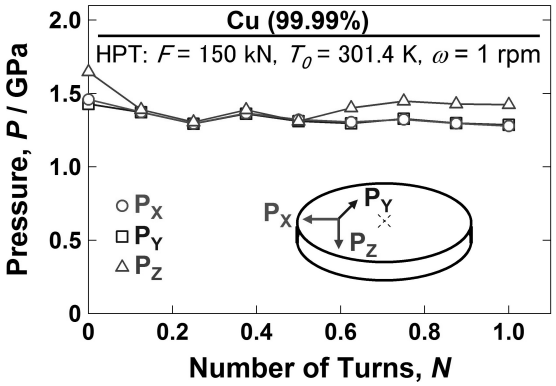

Fig. 7 Variation of average pressure in whole disc volume against number of turns at three different directions (X: radial, Y: transvers, Z: compression) obtained by FEM simulation for Cu processed by HPT under load of 150 kN.

Details of the FEM simulations for Cu sample processed under a load of 150 kN are shown in Figs. 7–9. It should be noted that the pressures (compression stresses) given in Fig. 7 are the mean pressures from the center to the periphery of the disc and the pressures given in Figs. 8 and 9 correspond to the surface and cross section of discs, respectively. Figures 7–9 indicate five important points. First, although the pressure in the compression direction (P_Z) is somewhat higher than the pressures in the radial direction (P_X) and the transverse direction (P_Y), the hydrostatic pressure in processing by HPT, $(P_X + P_Y + P_Z)/3$, can be reasonably considered isotropic ($P_X = P_Y = P_Z$). Second, the mean hydrostatic pressure is almost independent of the number of turns. Third, the pressure decreases with increasing the distance from the disc center as a consequence of the material flow into the burr region. Bridgman also employed the Hertz theory for classical elasticity and suggested that the pressure should be higher at the disc center when compared with the disc periphery[11]. Fourth, the pressure at the disc center is even higher than the nominal pressure calculated by $F/\pi R^2$. Myers *et al.* also reported similar results by calibration of pressure using the electrical resistivity measurements[40]. They suggested that this unusual

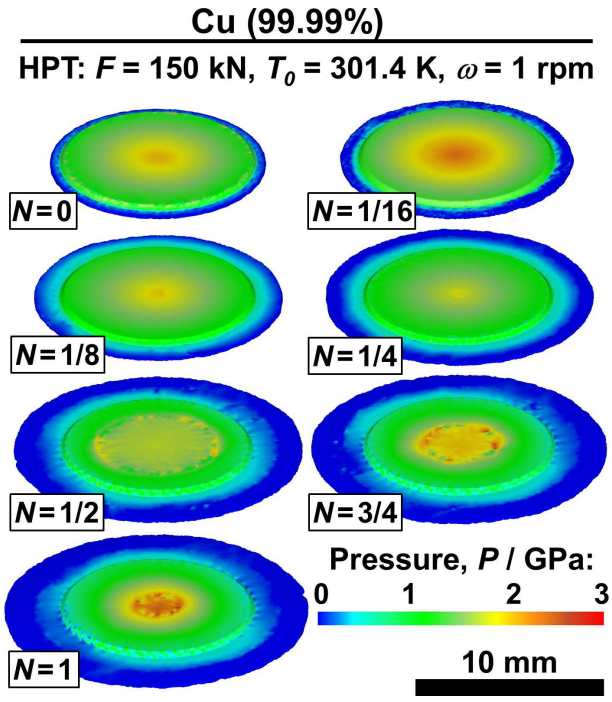

Fig. 8 Contours of pressure distribution on disc surface for Cu processed by HPT for different numbers of turns under load of 150 kN.

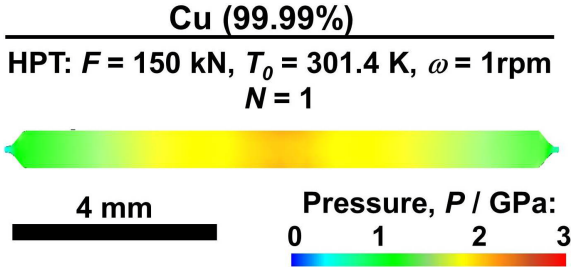

Fig. 9 Contour of pressure distribution on cross section of disc for Cu processed by HPT for $N = 1$ turn under load of 150 kN.

pressure multiplication can be avoided by increasing the disc diameter-to-thickness ratio[40]. Fifth, the pressure for a given distance from the disc center is reasonably uniform across the thickness.

Finally, it should be noted that the current experimental and simulation results were achieved for thin disc specimens processed between a pair of anvils with perfect alignment. If the alignment of two anvils is not adjusted well, the distribution of pressure can be changed significantly because of changes in the total contact area as well as because of changes in the flow behavior of material[39]. The pressure distribution can be even more non-uniform, if the thickness-to-diameter ratio of the disc increases[4,11,40].

5. Conclusions

In summary, the current study provides some experimental and FEM simulation results on the magnitude of real hydrostatic pressure during processing by HPT. The results show that the real hydrostatic pressure depends not only on the compressive load and the area of disc but also on the contact area between the upper and lower anvils (burr region) as well as on the distance from the disc center. The current results show that the calculation of pressure as the load over the initial area of the disc is the main reason for overestimation of phase-transition pressures during the HPT process.

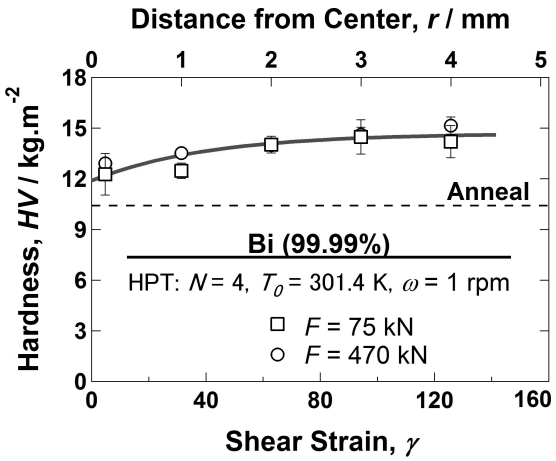

Fig. A.1 Vickers microhardness plotted against shear strain and distance from disc center for Bi samples processed by HPT for $N = 4$ turns under loads of 75 kN and 470 kN.

Acknowledgments

The authors would like to thank Prof. Kenji Higashida of Kyushu University for kind discussion. One of the authors (KE) acknowledges a grant from Kyushu University Interdisciplinary Programs in Education and Projects in Research Development (P&P) (No. 27513). This work was supported in part by the Grant-in-Aids from the MEXT, Japan (No. 22102004, No. 26220909 and No. 15K14183) and in part by the National Research Foundation of Korea (NRF), the Korean Government (MSIP) (No. 2014R1A2A1A10051322). The HPT process was carried out in the International Research Center on Giant Straining for Advanced Materials (IRC-GSAM) at Kyushu University.

Appendix

Figure A.1 shows the variation of hardness against shear strain γ ($\gamma = 2\pi rN/h$, r: distance from disc center, N: number of turns, h: disc thickness[1]) for Bi samples processed by HPT for $N = 4$ turns under loads of 75 kN and 470 kN. The hardness increases with increasing the shear strain and saturates to a steady state level of 14 Hv at large strains. The hardness-strain behaviors appear to be reasonably independent of the compressive load. It should be noted that similar to pure metals with low melting temperatures such as In, Sn, Pb and Zn, in which small changes in hardness occurs by HPT processing[38,41], Bi also exhibits small changes in hardness (hardness of annealed Bi was 10 Hv). The main difference between Bi and other metals with low melting temperatures is that Bi exhibits a slight hardening by HPT processing, whereas In, Sn, Pb and Zn exhibit a slight softening (below the hardness levels for the annealed samples) after processing by HPT.

Optical micrographs of Bi samples after (a) annealing at

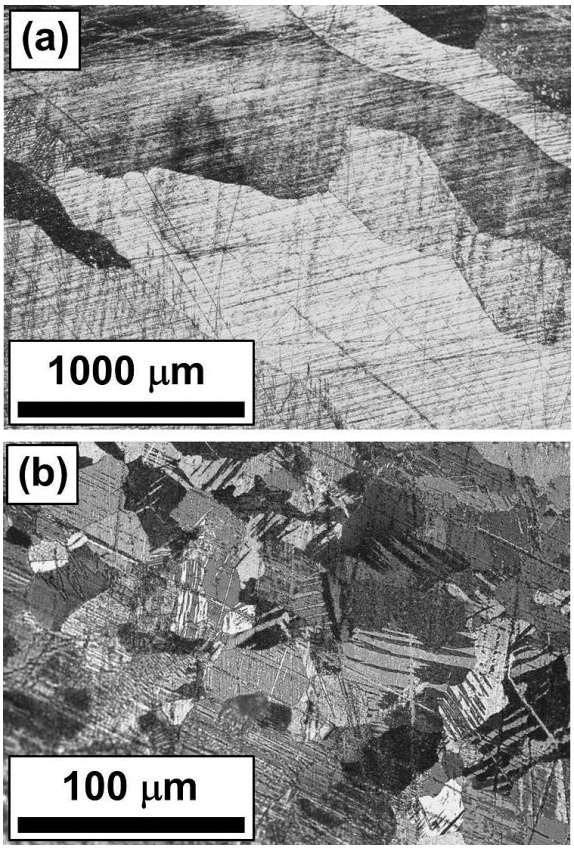

Fig. A.2 Microstructure of Bi observed using optical microscopy after (a) annealing at 493 K for 1 h and (b) HPT processing for $N = 4$ turns under a load of 470 kN taken at 4 mm away from disc center..

493 K for 1 h and (b) HPT processing for $N = 4$ turns under a load of 470 kN are shown in Fig. A.2. It is shown that the microstructure consists of large grains with an average grain size of ~1000 μm after annealing, while the average grain size decreases to ~20 μm after processing by HPT. Many twins can be seen in the sample processed by HPT. The presence of large fraction of these twins together with the non-compact rhombohedral crystal structure of Bi-I can be two possible reasons for the occurrence of slight hardening rather than expected softening in Bi during the HPT processing. It should be noted that the only phase that could be detected in this study after HPT processing under different loads was Bi-I. The absence of high-pressure phases in HPT-processed Bi is reasonable because Bi-II and Bi-III phases are not stable at ambient condition and they transform to Bi-I after releasing the pressure[11].

REFERENCES

1) R. Z. Valiev, R. K. Islamgaliev and I. V. Alexandrov: Prog. Mater. Sci. **45** (2000) 103–189.
2) R. Z. Valiev, Y. Estrin, Z. Horita, T. G. Langdon, M. J. Zehetbauer and Y. T. Zhu: JOM **58** (4) (2006) 33–39.
3) A. P. Zhilyaev and T. G. Langdon: Prog. Mater. Sci. **53** (2008) 893–979.
4) R. Pippan, S. Scheriau, A. Taylor, M. Hafok, A. Hohenwarter and A. Bachmaier: Annu. Rev. Mater. Res. **40** (2010) 319–43.
5) K. Edalati, S. Toh, Y. Ikoma and Z. Horita: Scr. Mater. **65** (2011) 974–977.
6) V. I. Levitas, Y. Ma, E. Selvi, J. Wu and J. A. Patten: Phys. Rev. B **85** (2012) 054114.
7) M. T. Perez-Prado, A. A. Gimazov, O. A. Ruano, M. E. Kassner and A.P. Zhilyaev: Scr. Mater. **58** (2008) 219–222.
8) Y. Ivanisenko, A. Kilmametov, H. Rosner and R. Z. Valiev: Int. J. Mater. Res. **99** (2008) 36–41.
9) B. B. Straumal, A. S. Gornakova, O. B. Fabrichnaya, M. J. Kiregel, A. A. Mazilkin, B. Baretzky, A. M. Gusak and S. V. Dobatkin: High Temp. Mater. Proc. **31** (2012) 339–350.
10) N. Q. Chinh, R. Z. Valiev, X. Sauvage, G. Varga, K. Havancsak, M. Kawasaki, B. B. Straumal and T. G. Langdon: Adv. Eng. Mater. **16** (2014) 1000–1009.
11) P. W. Bridgman: Phys. Rev. **48** (1935) 825–847.
12) K. Edalati, R. Miresmaeili, Z. Horita, H. Kanayama and R. Pippan: Mater. Sci. Eng. A **528** (2011) 7301–7305.
13) R. B. Figueiredo, P. H. R. Pereira, M. T. P. Aguilar, P. R. Cetlin and T. G. Langdon: Acta Mater. **60** (2012) 3190–3198.
14) P. W. Bridgman: Proc. Am. Acad. Arts. Sci. **83** (1954) 151–190.
15) P. W. Bridgman and I. Simon: J. Appl. Phys. **24** (1953) 405–413.
16) F. L. Vereshchagin and V. A. Shapochkin: Fiz. Met. Metalloved. **9** (1960) 258–264.
17) V. A. Shabashov: Nanostruct. Mater. **6** (1995) 711–714.
18) B. Efros, V. Pilyugin, A. Patselov, S. Gladkovskii, N. Efros, L. Loladze and V. Varyukhin: Mater. Sci. Eng. A **503** (2009) 114–117.
19) K. Edalati, E. Matsubara and Z. Horita: Metall. Mater. Trans. A **40** (2009) 2079–2086.
20) K. Edalati, Z. Horita, S. Yagi and E. Matsubara: Mater. Sci. Eng. A **523** (2009) 277–281.
21) K. Edalati and Z. Horita: Mater. Sci. Eng. A **652** (2016) 325–352.
22) V. V. Aksenenkov, V. D. Blank, Y. S. Konyayev, A. I. Kunzetsov and E. I. Estrin: Phys. Met. Metallogr. **57** (1984) 159–162.
23) V. Blank, M. Popov, S. Buga, V. Davydov, V. N. Denisov, A. N. Ivlev, B. N. Mavrin, V. Agafonov, R. Ceolin, H. Szwarc and A. Rassat: Phys. Lett. A **188** (1994) 281–286.
24) S. K. Sikka, Y. K. Vohra and R. Chidambaram: Prog. Mater. Sci. **27** (1982) 245–310.
25) P. W. Bridgman: Proc. Am. Acad. Arts Sci. **76** (1948) 71–87.
26) J. C. Jamieson: Science **140** (1963) 72–73.
27) V. A. Zilbershtein, G. I. Nosova and E. I. Estrin: Phys. Met. Metallogr. **35** (1973) 128–133.
28) A. R. Kilmametov, A. V. Khristoforova, G. Wilde and R. Z. Valiev: Z. Kristallogr. Suppl. **26** (2007) 339–344.
29) Y. Todaka, J. Sasaki, T. Moto and M. Umemoto: Scr. Mater. **59** (2008) 615–618.
30) M. Shirooyeh, J. Xu and T. G. Langdon: Mater. Sci. Eng. A **614** (2014) 223–231.
31) A. V. Sergueeva, V. V. Stolyarov, R. Z. Valiev and A. K. Mukherjee: Scr. Mater. **45** (2001) 747–752.
32) Y. J. Chen, Y. J. Li, J. C. Walmsley, N. Gao, H. J. Roven, M. J. Starnik and T.G. Langdon: J. Mater. Sci. **47** (2012) 4838–4844.
33) C. T. Wang, A. G. Fox and T. G. Langdon: J. Mater. Sci. **49** (2014) 6558–6564.
34) R. G. Hennig, D. R. Trinkle, J. Bouchet, S. G. Srinivasan, R. C. Albers and J. W. Wilkins: Nature Mater. **4** (2005) 129–133.
35) P. W. Bridgman: Rev. Mod. Phys. **18** (1946) 1–93.
36) K. Edalati, T. Fujioka and Z. Horita: Mater. Sci. Eng. A **497** (2008) 168–173.
37) D. J. Lee, E. Y. Yoon, D. H. Ahn, B. H. Park, H. W. Park, L. J. Park, Y. Estrin and H. S. Kim: Acta Mater. **76** (2014) 281–293.
38) K. Edalati and Z. Horita: Mater. Sci. Eng. A **528** (2011) 7514–7523.
39) Y. Huang, M. Kawasaki and T. G. Langdon: J. Mater. Sci. **49** (2014) 3146–3157.
40) M. B. Myers, F. Dachille and R. Roy: Rev. Sci. Instrum. **34** (1963) 401–402.
41) B. Srinivasarao, A. P. Zhilyaev, T. G. Langdon and M. T. Perez-Prado: Mater. Sci. Eng. A **562** (2013) 196–202.